Polarization Calibration of the VLA Analog Sum

Mark M. McKinnon

March 12, 1990

I. Introduction.

A polarization calibration scheme for the analog sum is needed not only to calibrate observations, but also to analyze the performance of new detection equipment, specifically, the High Time Resolution Processor (HTRP). Since a phased array emulates a single dish telescope, the procedure I present for the polarization calibration of a point source observation is similar to that presented by Stinebring (1982) for the Arecibo telescope. The major differences in the methods are the summing of signals from separate antennas and the inclusion of the instrumental polarization phase for absolute polarization angle calculations. My analysis also differs from traditional calibration schemes (Stinebring, 1982 and Conway and Kronberg, 1969) by the introduction of a complex gain to account for the non-ideality of the detectors. The procedure I propose may be of use to other phased array observations (e.g. VLBI) and single dish observations as well as the HTRP.

II. Review of Stokes Parameters.

To define the terminology used in this memorandum, I shall briefly review the definitions and properties of Stokes parameters. Consider a monochromatic, electromagnetic wave which can be decomposed into orthogonal right (RCP) and left (LCP) circularly polarized components. Although the actual signals measured are broad band as opposed to monochromatic, the results of the single frequency component analysis may be extended to the broad band case because the individual frequency components may be considered independent of each other. The polarization components are defined by the equations

$$\mathrm{E_R} = E_r \exp(i(\omega t - \theta)) \tag{1}$$

$$\mathrm{E_L} = E_l \exp(i\omega t) \tag{2}$$

where θ is the difference in phase between the two polarized components. The bold face characters (e.g. $\mathrm{E_R}$) denote complex quantities, and script characters generally represent real quantities.

From Figures 1 and 2, one sees that the position angle (θ) changes with source position. The position angle is the angle between the source linear polarization vector, P, and the vertical axis of an altitude-azimuth mounted telescope. At transit, the position angle is equal to the true polarization angle, ϕ. The sign convention for ϕ is positive as measured from north through east. The parallactic angle, β, is the angle between the source "axis" and the telescope axis. The parallactic angle is negative at negative hour angles (HA) and positive at positive hour angles. Thus the left side of Figure 1 corresponds to east (negative HA and negative β) and the right side corresponds to west (positive HA and positive β). As seen in Figure 2, the apparent polarization, $|\mathrm{P}|\cos\theta$, varies as a cosine in

Figure 1: Rotation of Source Polarization Vector

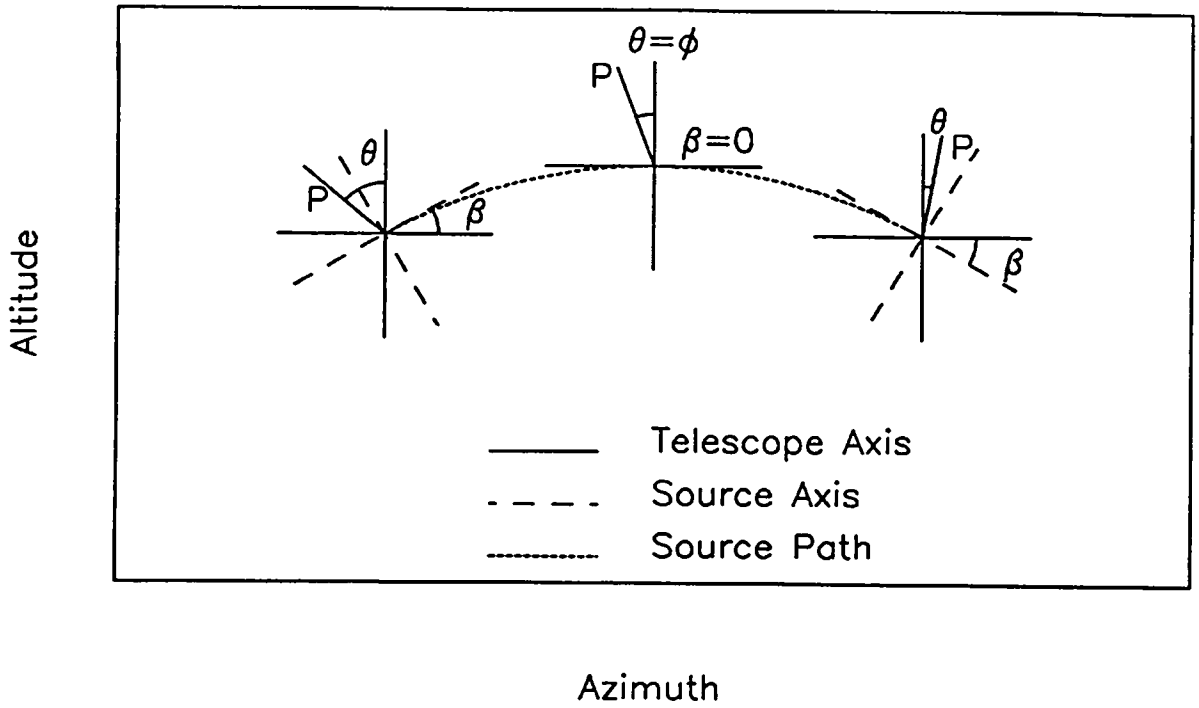

Figure 2: Polarization Dependence upon Parallactic Angle

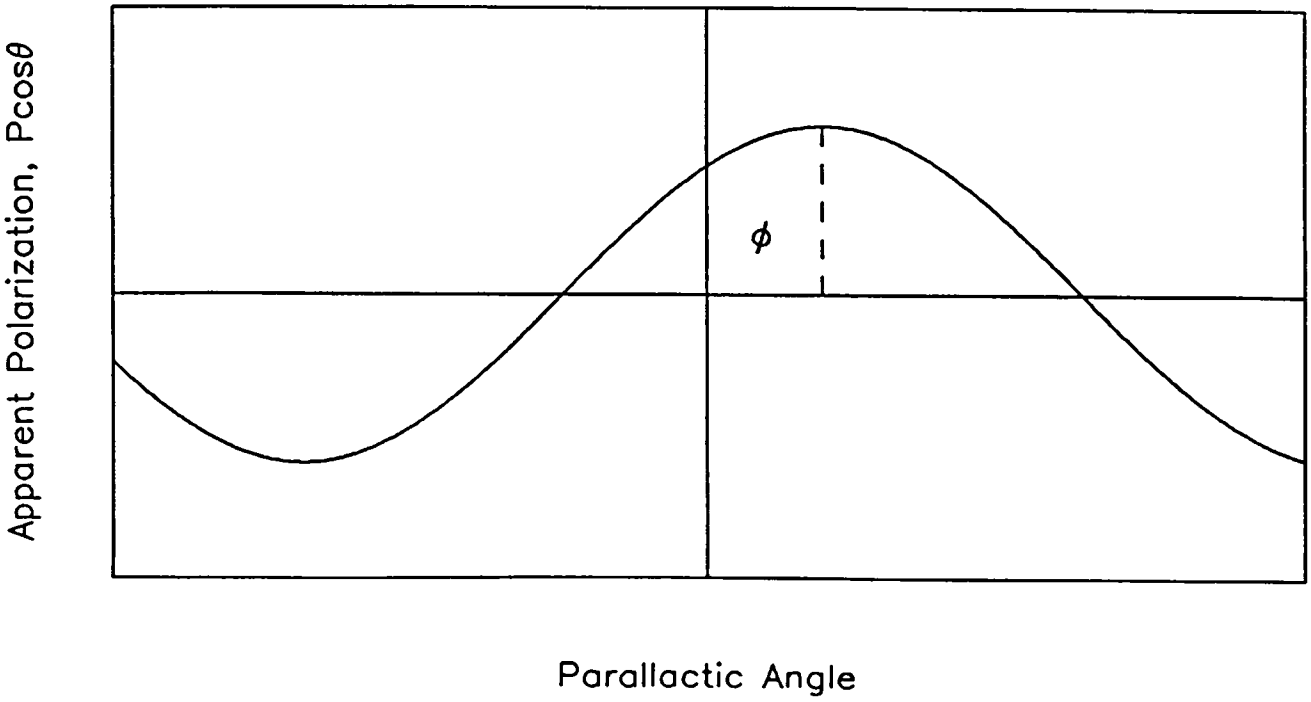

parallactic angle with a phase offset equal to the source polarization angle. From Conway and Kronberg, 1969, (or Kraus, 1966) "if the position angle of the source varies with respect to the instrument by an angle ψ, the phase of the true polarization alters by 2ψ". Therefore, θ shall be defined as $\theta = 2(\beta - \phi)$ because this definition gives positive ϕ when measured from north through east (see Figures 1 and 2).

The Stokes parameters for the electromagnetic wave are (Jackson, 1975)

$$I = \mathrm{E_L E_L^*} + \mathrm{E_R E_R^*} = E_l^2 + E_r^2 \tag{3}$$

$$Q = 2E_l E_r \cos\theta = \mathrm{E_L^* E_R} + \mathrm{E_L E_R^*} \tag{4}$$

$$U = 2E_l E_r \sin\theta = i(\mathrm{E_L^* E_R} - \mathrm{E_L E_R^*}) \tag{5}$$

$$V = \mathrm{E_L E_L^*} - \mathrm{E_R E_R^*} = E_l^2 - E_r^2 \tag{6}$$

Recall that the quantities in equations 3 through 6 are time averages. One may also write $\mathrm{E_R E_R^*}, \mathrm{E_L E_L^*}, \mathrm{E_L^* E_R}$, and $\mathrm{E_L E_R^*}$ in terms of I, Q, U, and V.

$$\mathrm{E_L E_L^*} = (I + V)/2 \tag{7}$$

$$\mathrm{E_R E_R^*} = (I - V)/2 \tag{8}$$

$$\mathrm{E_L E_R^*} = (Q + iU)/2 \tag{9}$$

$$\mathrm{E_L^* E_R} = (Q - iU)/2. \tag{10}$$

III. Parallel and Cross Products of the Analog Sum IF's.

The signal received by an antenna feed of circular polarization cannot be accurately represented by equations 1 and 2. The actual signal received in a single IF of an antenna is corrupted by cross-talk from the IF of opposite polarization (Conway and Kronberg, 1969). Correcting equations 1 and 2 for cross-talk at the jth antenna gives

$$\mathrm{E'_{jR}} = \frac{\mathrm{E_R} + \mathrm{E_L}\epsilon_{\mathrm{jR}}}{(1 + \epsilon_{jR}^2)^{1/2}} \tag{11}$$

$$\mathrm{E'_{jL}} = \frac{\mathrm{E_L} + \mathrm{E_R}\epsilon_{\mathrm{jL}}}{(1 + \epsilon_{jL}^2)^{1/2}} \tag{12}$$

The terms $\epsilon_{\mathrm{jL}} = \epsilon_{jL} e^{i\phi_{jL}}$ and $\epsilon_{\mathrm{jR}} = \epsilon_{jR} e^{-i\phi_{jR}}$ are complex leakage factors, and the denominator serves as a normalization factor. The output voltages of the jth antenna in the array are proportional to $\mathrm{E'_R}$ and $\mathrm{E'_L}$ by the complex gains $\mathrm{G_{jR}}$ and $\mathrm{G_{jL}}$, respectively.

$$V_{jR} = G_{jR} E'_R \tag{13}$$

$$V_{jL} = G_{jL} E'_L \tag{14}$$

The data path of an antenna signal is as follows for the HTRP system. The analog sum of the VLA adds the individual antenna signals for a single IF. The broad band summed signal is subdivided into narrower subbands by the videoconverters in the Mk III filter bank. Selected videoconverter outputs are multiplied by an appropriate complex conjugate to generate the parallel products, RR and LL, and the cross products, RL and LR. The parallel and cross products are ultimately used to calculate the source Stokes parameters.

The multiplying polarimeter creates the parallel and cross products as shown in Figure 3 for an ideal case. In the particular case of the HTRP, the RCP polarization component is shifted by +90 degrees to generate the RL cross product. The addition of a 90 degree phase shift is equivalent to multiplying by $e^{i\pi/2} = i = \sqrt{-1}$. One can show in the algebra that RL and LR do not depend upon which polarization component is phase shifted or complex conjugated; however, the sign of RL does depend upon the sign of the phase shift.

The detected output of the analog sum in RCP for N antennas in the array is

$$RR = B_{RR}(A_R \sum_{j=1}^{N} V_{jR})(A_R \sum_{k=1}^{N} V_{kR})^* = B_{RR} A_R^2 \sum_{j}^{N} \sum_{k}^{N} (V_{jR} V_{kR}^*). \tag{15}$$

A_R is the complex gain of the videoconverter, and $B_{RR} = B_{RR} e^{i\psi_{RR}}$ is the complex gain of the RR detector. Different summation indices (j, k) may be used in equation 15 because once the antenna voltages are summed, all individual antenna information is lost. Justification for the detector gain term will be given in Section VI. Similarly, the remaining complex conjugated products are

$$LL = B_{LL} A_L^2 \sum_{j}^{N} \sum_{k}^{N} (V_{jL} V_{kL}^*) \tag{16}$$

$$LR = B_{LR} A_R A_L^* \sum_{j}^{N} \sum_{k}^{N} (V_{kL}^* V_{jR}) \tag{17}$$

$$RL = i B_{RL} A_R A_L^* \sum_{j}^{N} \sum_{k}^{N} (V_{kL}^* V_{jR}). \tag{18}$$

Carrying out the multiplication and substituting equations 7 through 10, one finds

$$LL = \frac{1}{2} B_{LL} A_L^2 \sum_{j}^{N} \sum_{k}^{N} \left\{ \frac{G_{jL} G_{kL}^*}{\sqrt{(1+\epsilon_{jL}^2)(1+\epsilon_{kL}^2)}} [I(1 + \epsilon_{jL} \epsilon_{kL}^*) \right.$$

Figure 3: Multiplying Polarimeter

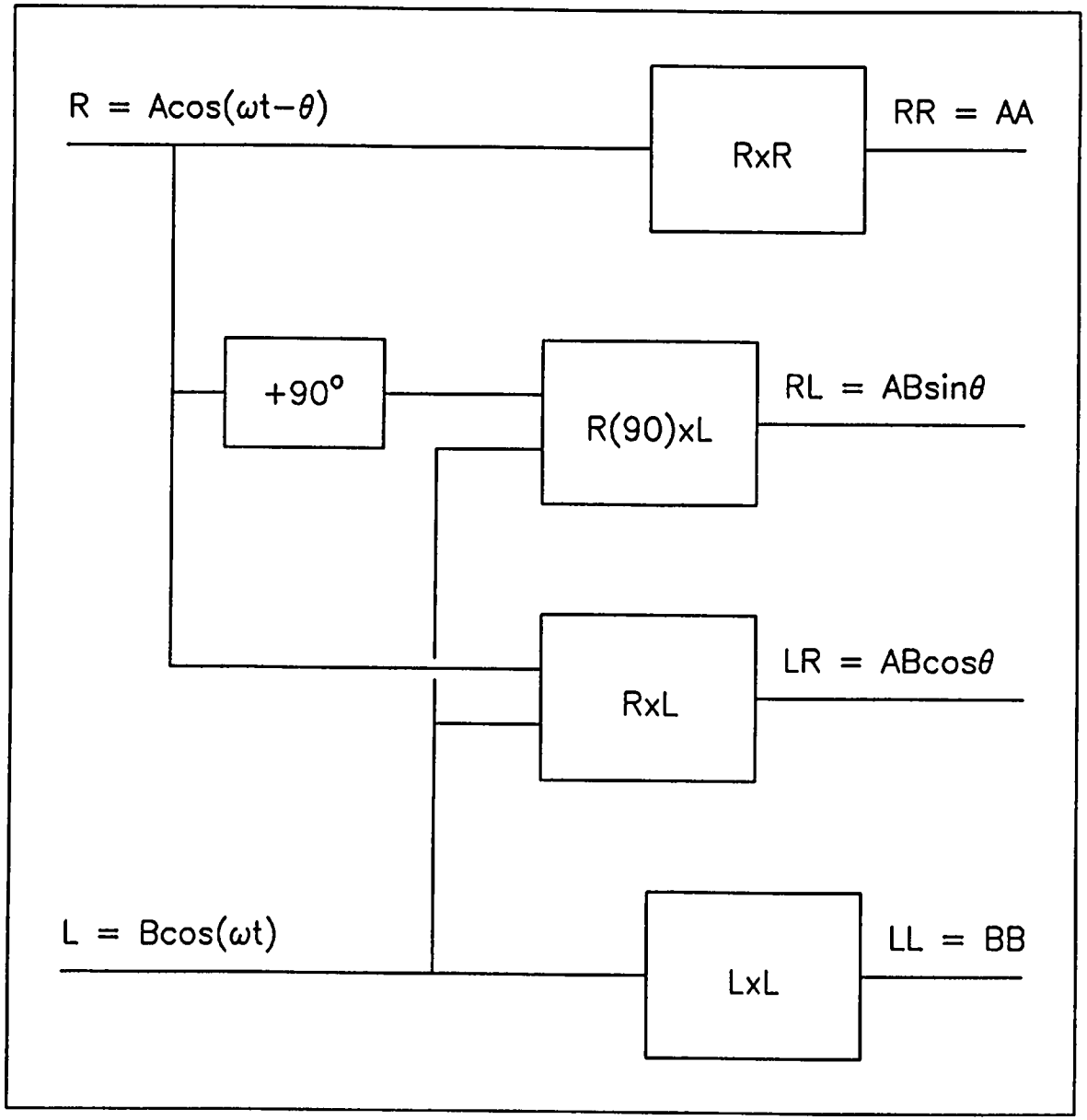

$$+ V(1 - \epsilon_{\mathrm{jL}}\epsilon^*_{\mathrm{kL}}) + (Q - iU)\epsilon_{\mathrm{jL}} + (Q + iU)\epsilon^*_{\mathrm{kL}}\Big]\Big\} \tag{19}$$

$$\mathrm{RR} = \frac{1}{2}\mathrm{B_{RR}}A_R^2 \sum_j^N \sum_k^N \Big\{ \frac{\mathrm{G_{jR}G^*_{kR}}}{\sqrt{(1+\epsilon_{jR}^2)(1+\epsilon_{kR}^2)}} \big[I(1 + \epsilon_{\mathrm{jR}}\epsilon^*_{\mathrm{kR}})$$

$$- V(1 - \epsilon_{\mathrm{jR}}\epsilon^*_{\mathrm{kR}}) + (Q + iU)\epsilon_{\mathrm{jR}} + (Q - iU)\epsilon^*_{\mathrm{kR}}\big]\Big\} \tag{20}$$

$$\mathrm{RL} = \frac{i}{2}\mathrm{A_R A^*_L B_{RL}} \sum_j^N \sum_k^N \Big\{ \frac{\mathrm{G_{kL}G^*_{jR}}}{\sqrt{(1+\epsilon_{kL}^2)(1+\epsilon_{jR}^2)}} \big[Q(1 + \epsilon^*_{\mathrm{kL}}\epsilon_{\mathrm{jR}})$$

$$- iU(1 - \epsilon^*_{\mathrm{kL}}\epsilon_{\mathrm{jR}}) + I(\epsilon^*_{\mathrm{kL}} + \epsilon_{\mathrm{jR}}) + V(\epsilon_{\mathrm{jR}} - \epsilon^*_{\mathrm{kL}})\big]\Big\} \tag{21}$$

$$\mathrm{LR} = \frac{1}{2}\mathrm{A_R A^*_L B_{LR}} \sum_j^N \sum_k^N \Big\{ \frac{\mathrm{G_{jR}G^*_{kL}}}{\sqrt{(1+\epsilon_{jR}^2)(1+\epsilon_{kL}^2)}} \big[Q(1 + \epsilon_{\mathrm{jR}}\epsilon^*_{\mathrm{kL}})$$

$$- iU(1 - \epsilon_{\mathrm{jR}}\epsilon^*_{\mathrm{kL}}) + I(\epsilon_{\mathrm{jR}} + \epsilon^*_{\mathrm{kL}}) + V(\epsilon_{\mathrm{jR}} - \epsilon^*_{\mathrm{kL}})\big]\Big\} \tag{22}$$

Equations 19 through 22 may be greatly simplified by assuming the magnitudes of the complex leakage factors are much less than one ($\epsilon << 1$); therefore, terms which are second order in ϵ are negligible. If the source linear polarization is defined as $\mathrm{P} = Pe^{i\theta} = Q + iU$, equation 20 simplifies to

$$\mathrm{RR} = \frac{1}{2}A_R^2\mathrm{B_{RR}}\big[(I - V)\sum_j^N \sum_k^N (\mathrm{G_{jR}G^*_{kR}}) + \mathrm{P}\sum_j^N \sum_k^N (\mathrm{G_{jR}G^*_{kR}}\epsilon_{\mathrm{jR}})$$

$$+ \mathrm{P}^* \sum_j^N \sum_k^N (\mathrm{G_{jR}G^*_{kR}}\epsilon^*_{\mathrm{kR}})\big] \tag{23}$$

Looking at the summations of the gain terms, one notices the summations are proportional to the averages of their arguments.

$$\sum_j^N \sum_k^N (\mathrm{G_{jR}G^*_{kR}}) = N^2\langle \mathrm{G_{jR}}\rangle\langle \mathrm{G^*_{kR}}\rangle \tag{24}$$

$$\sum_{j}^{N}\sum_{k}^{N}(\mathrm{G_{jR}G^*_{kR}}\epsilon_{\mathrm{jR}}) = N^2\langle \mathrm{G^*_{kR}}\rangle\langle G_{jR}\epsilon_{jR}\rangle \tag{25}$$

If the leakage terms are independent of the gains, the covariance of $\mathrm{G}\epsilon$ is $\mathrm{Cov}(\mathrm{G_{jR}}\epsilon_{\mathrm{jR}}) = \langle \mathrm{G_{jR}}\epsilon_{\mathrm{jR}}\rangle - \langle \mathrm{G_{jR}}\rangle\langle\epsilon_{\mathrm{jR}}\rangle = 0$. Simply stated, the zero covariance stipulates that a change in antenna gain does not produce a change in the antenna IF leakage. The zero covariance allows one to factor out the average gain in equation 23. The expression for RR reduces to

$$\mathrm{RR} = \frac{1}{2}A_R^2\mathrm{B_{RR}}N^2|\langle \mathrm{G_{jR}}\rangle|^2[I - V + \mathrm{P}\langle\epsilon_{\mathrm{jR}}\rangle + \mathrm{P}^*\langle\epsilon^*_{\mathrm{kR}}\rangle] \tag{26}$$

If we define $\langle \mathrm{G_{jR}}\rangle = G_R e^{i\psi_R}$ and $\langle\epsilon_{\mathrm{kR}}\rangle = \epsilon_R e^{i\phi_R}$, and recall that the sum of the complex conjugates is the complex conjugate of the sum (i.e. $\langle\epsilon^*_{\mathrm{kR}}\rangle = \langle\epsilon_{\mathrm{kR}}\rangle^*$), RR simplifies to

$$\mathrm{RR} = \frac{1}{2}\mathrm{B_{RR}}A_R^2G_R^2N^2[(I - V) + 2P\epsilon_R\cos(\theta - \phi_R)] \tag{27}$$

because for any complex number $\mathrm{z} = ze^{i\theta}, \mathrm{z} + \mathrm{z}^* = 2z\cos\theta$. Since the signals actually recorded are *real* signals, the signal recorded for RR is

$$RR = Re[\mathrm{RR}] = \frac{1}{2}A_R^2G_R^2N^2B_{RR}\cos\psi_{RR}[(I - V) + 2P\epsilon_R\cos(\theta - \phi_R)] \tag{28}$$

Similarly for LL one finds

$$LL = Re[\mathrm{LL}] = \frac{1}{2}A_L^2G_L^2N^2B_{LL}\cos\psi_{LL}[(I + V) + 2P\epsilon_L\cos(\theta - \phi_L)] \tag{29}$$

where $\langle\epsilon_{\mathrm{jL}}\rangle = \epsilon_L e^{i\phi_L}, \langle \mathrm{G_{jL}}\rangle = G_L e^{i\phi_L}$ and $\mathrm{B_{LL}} = B_{LL}e^{i\phi_{LL}}$. Using the assumptions of $\epsilon << 1$ and $\mathrm{Cov}(\mathrm{G}\epsilon) = 0$ for RL, one finds

$$\mathrm{RL} = \frac{i}{2}\mathrm{B_{RL}A_RA^*_L}N^2\langle \mathrm{G_{jR}}\rangle\langle \mathrm{G^*_{kL}}\rangle[\mathrm{P}^* + I(\langle\epsilon_{\mathrm{jR}}\rangle + \langle\epsilon^*_{\mathrm{kL}}\rangle) + V(\langle\epsilon_{\mathrm{jR}}\rangle - \langle\epsilon^*_{\mathrm{kL}}\rangle)] \tag{30}$$

Next, define sum and difference vectors as

$$\mathrm{s} = \sigma e^{i\psi_+} = \langle\epsilon_{\mathrm{jR}}\rangle + \langle\epsilon^*_{\mathrm{kL}}\rangle \tag{31}$$

$$\mathrm{d} = \delta e^{i\psi_-} = \langle\epsilon_{\mathrm{jR}}\rangle - \langle\epsilon^*_{\mathrm{kL}}\rangle \tag{32}$$

and let $\mathrm{A_RA_L} = A_RA_Le^{i\psi_A}$ such that $\mathrm{A_RA_L}\langle \mathrm{G_{jR}}\rangle\langle \mathrm{G^*_{kL}}\rangle = A_RA_LG_RG_Le^{i\psi}$. The angle $\psi = \psi_R - \psi_L + \psi_A$ is the fundamental, instrumental contribution to the polarization angle. For those familiar with interferometric polarization calibration at the VLA, ψ is analogous to, but not the same as, the phase correction applied in the program POLCAL. RL becomes

$$\mathrm{RL} = \frac{i}{2} N^2 A_R A_L G_R G_L B_{RL} e^{i\psi_{RL}} e^{i\psi} [\mathrm{P}^* + I\mathrm{s} + V\mathrm{d}] \tag{33}$$

The recorded signal is the real part of RL.

$$RL = Re[\mathrm{RL}] = \frac{1}{2} A_R A_L G_R G_L B_{RL} N^2 [P \sin(\theta - \psi - \psi_{RL})$$

$$- I\sigma \sin(\psi_+ + \psi + \psi_{RL}) - V\delta \sin(\psi_- + \psi + \psi_{RL})] \tag{34}$$

Likewise, the recorded signal for LR becomes

$$LR = Re[\mathrm{LR}] = \frac{1}{2} A_R A_L G_R G_L B_{LR} N^2 [P \cos(\theta - \psi - \psi_{LR})$$

$$+ I\sigma \cos(\psi_+ + \psi + \psi_{LR}) + V\delta \cos(\psi_- + \psi + \psi_{LR})] \tag{35}$$

The implications of the expressions for RR, LL, RL, and LR are as follows:

1. A plot of LL or RR versus parallactic angle should produce a sinusoid with a constant offset. The offset will be proportional to $I \pm V$, and the amplitude of the sinusoid will be proportional to the linear polarization. For sources of small linear polarization and for instruments of very good design ($\epsilon \approx 0$), the LL and RR output will be constant with parallactic angle.

2. A plot of LR or RL versus parallactic angle should produce a sinusoid with a constant offset. The offset depends upon the source Stokes I and V, and the amplitude of the sinusoid will be proportional to the linear polarization. For instruments of very good design ($\sigma, \delta \approx 0$), there will be very little offset.

3. If the detectors are ideally designed ($B_{LR} = B_{RL} = 1$ and $\psi_{RL} = \psi_{LR} = 0$), the gain products of RL should equal that of LR, and the sinusoid of RL should be exactly 90 degrees out of phase with that of LR. LR and RL should be offset from true cosines and sines, respectively, by the same phase.

4. The sign of the constant offset in RL and LR depends upon the sign of the instrumental phases ($\psi_+, \psi_-, \psi_{RL}, \psi_{LR}$, and ψ) and the sense of circular polarization.

5. The sign of the constant offset in RR and LL is always non-negative.

6. When performing observations for polarization calibration, it is imperative that the number of antennas in the array remains constant (N^2 = constant).

A good check on the preceding analysis is to verify that it agrees with that of Stinebring for a single dish telescope. The simplest case is one in which the detectors are ideal. Additionally, if one is not interested in absolute polarization angle calibration, one may arbitrarily set the instrumental polarization, ψ, to zero. When ψ is set to zero, one can only

make quantitative statements about the *changes* in source polarization angle for different observations provided the gains remain constant between observations. This special case is also applicable to observations in which one is only interested in the magnitudes of I, V, and P. By observing a calibrator of little or no polarization ($V \approx P \approx 0$), one may determine the gain products in the expressions for RR and LL (equations 28 and 29, respectively). The gain products may be applied to the signals from a source of unknown polarization provided the instrumentation is linear in its reponse. Assuming linearity and after dividing by the appropriate gain products, the gain calibrated parallel products become

$$\mathrm{RR_c} = I - V + \mathrm{P}\langle\epsilon_{\mathrm{jR}}\rangle + \mathrm{P}^*\langle\epsilon^*_{\mathrm{kR}}\rangle \tag{36}$$

$$\mathrm{LL_c} = I + V + \mathrm{P}\langle\epsilon_{\mathrm{kL}}{}^*\rangle + \mathrm{P}^*\langle\epsilon_{\mathrm{jL}}\rangle \tag{37}$$

The measured Stokes I and V are

$$I_c = \frac{1}{2}(RR_c + LL_c) = \frac{1}{2}(2I + \mathrm{Ps} + \mathrm{P}^*\mathrm{s}^*) = I + P\sigma\cos(\theta + \psi_+) \tag{38}$$

$$V_c = \frac{1}{2}(LL_c - RR_c) = V - P\delta\cos(\theta + \psi_-) \tag{39}$$

The gain products calculated for the parallel products may be applied to the cross products. The gain calibrated cross products become

$$RL = P\sin\theta - I\sigma\sin\psi_+ - V\delta\sin\psi_- \tag{40}$$

$$LR = P\cos\theta + I\sigma\cos\psi_+ + V\delta\cos\psi_- \tag{41}$$

The first term in equation 40 is Stokes U, and the first term in equation 41 is Stokes Q. Interpreting equations 40 and 41 as expressions for measured Stokes U and Q gives

$$U_c = U - I\sigma\sin\psi_+ - V\delta\sin\psi_- \tag{42}$$

$$Q_c = Q + I\sigma\cos\psi_+ + V\delta\cos\psi_- \tag{43}$$

Equations 38, 39, 42, and 43 agree exactly with the Stinebring expressions for the measured Stokes parameters provided one accounts for the differences in definitions of sum and difference vectors. As Stinebring shows, it is computationally convenient to express the measured and actual Stokes parameters as four-element vectors. The vectors are proportional to one another by a four-by-four matrix. The matrix elements are determined by equations 38, 39, 42, and 43. I refer the reader to Stinebring for details of the matrix as I prefer to work with the parallel and cross products.

IV. Recipe for Polarization Calibration.

A. Observe blank sky to determine the instrumental system noise. The magnitudes of the blank sky RR and LL signals will be considerable, and the magnitudes of RL and LR will be small. LR will typically be larger than RL because correlated signals (e.g. waveguide cycle at the VLA) exist in the IFs of opposite polarization.

B. Observe a calibrator of known flux. Ideally the calibrator should be unpolarized, but as will be shown in Section V, the instrumental contribution to RR and LL is small enough to ignore. This allows steps B and D to be combined.

C. Subtract the signals in A from the corresponding signals in B to calculate the gains for the parallel products. Applying the gains to other source observations normalizes the source flux to that of the flux calibrator.

D. Observe a calibrator of known polarized flux and polarization angle at different times near transit of the calibrator. The observations near transit provide a large variation in parallactic angle. An appropriate sinusoid fit to the blank sky corrected RL and LR data allows one to calculate the cross product gains and the instrumental polarization phase.

E. Apply the gain terms and instrumental polarization phase to the blank sky corrected data of a source of unknown polarization properties. Multiply the gain corrected data by the calibrator flux to calculate the source flux.

V. Results.

The recipe in Section IV was applied to HTRP observations conducted on February 14, 1990. IF's A and D of the VLA were phased at center frequencies of 8515MHz and bandwidths of 50MHz. Noise tube switching was turned off. The high frequency was used to avoid Faraday rotation due to the earth's ionosphere. The VLA was in its largest configuration (A). Since weather conditions were less than ideal, large telescope baselines and high observing frequency contributed to atmospheric phase stability problems. The upper sidebands of two Mk III videoconverters were configured for 1MHz bandwidths and local oscillator (LO) frequencies of 160MHz. The LO setting corresponds to a sky frequency of 8529.5MHz. Over the course of the observation, the number of antennas in the array remained constant. 3C286 was used as both a flux calibrator and a polarization calibrator.

Figures 4a and 4b are plots of equations 28 and 29, respectively, versus parallactic angle for 3C286. The parallactic angle was calculated based upon the latitude and longitude of the center of the array. The data have been corrected for gain, and are normalized to the flux of 3C286. Each data point is the average of 6000 samples, and corresponds to about 15 minutes of time. If any sinusoidal variation is present, its amplitude is below the two percent level. The scatter in the data is largely due to the atmosphere phase instability. Similar plots of X-band data collected in the D array configuration show much less scatter. The plots verify implications #1 and #5 in Section III, and indicate ϵ_R and ϵ_L are very small.

Figures 4c and 4d are plots of equations 34 and 35, respectively, versus parallactic angle for 3C286. The data has been corrected for the gains of the parallel products, but not the gains of the cross product detectors. The equations in the upper right hand corners of the

Figure 4a: Right Circular Polarization (RR) of 3C286

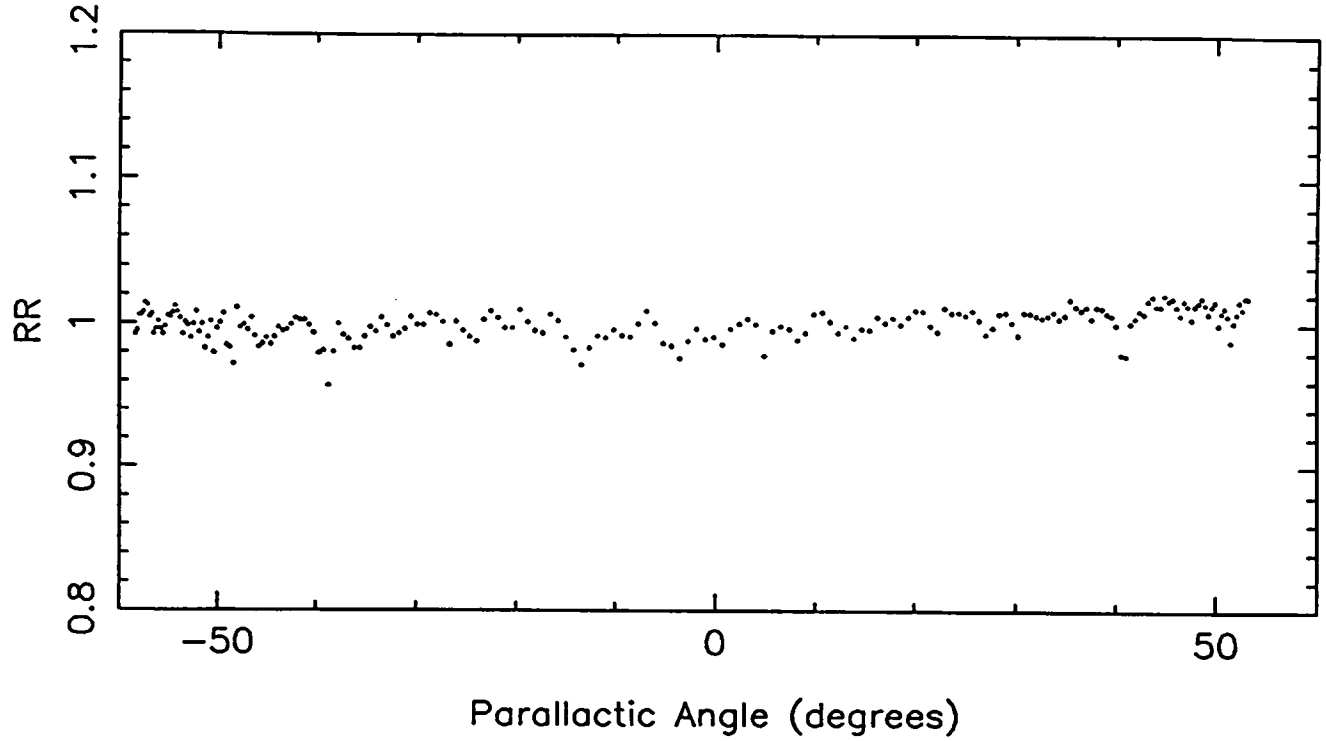

Figure 4b: Left Circular Polarization (LL) of 3C286

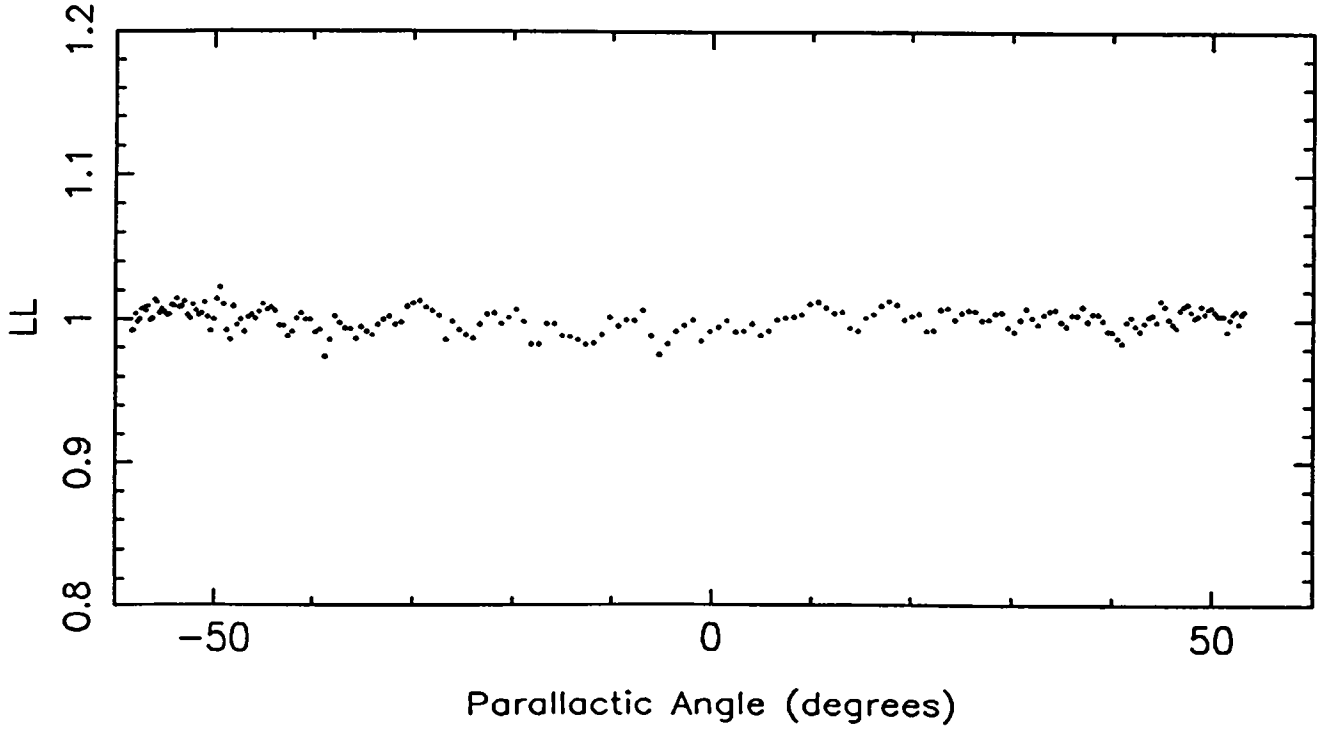

Figure 4c: Imaginary Part of Cross Products (RL) for 3C286

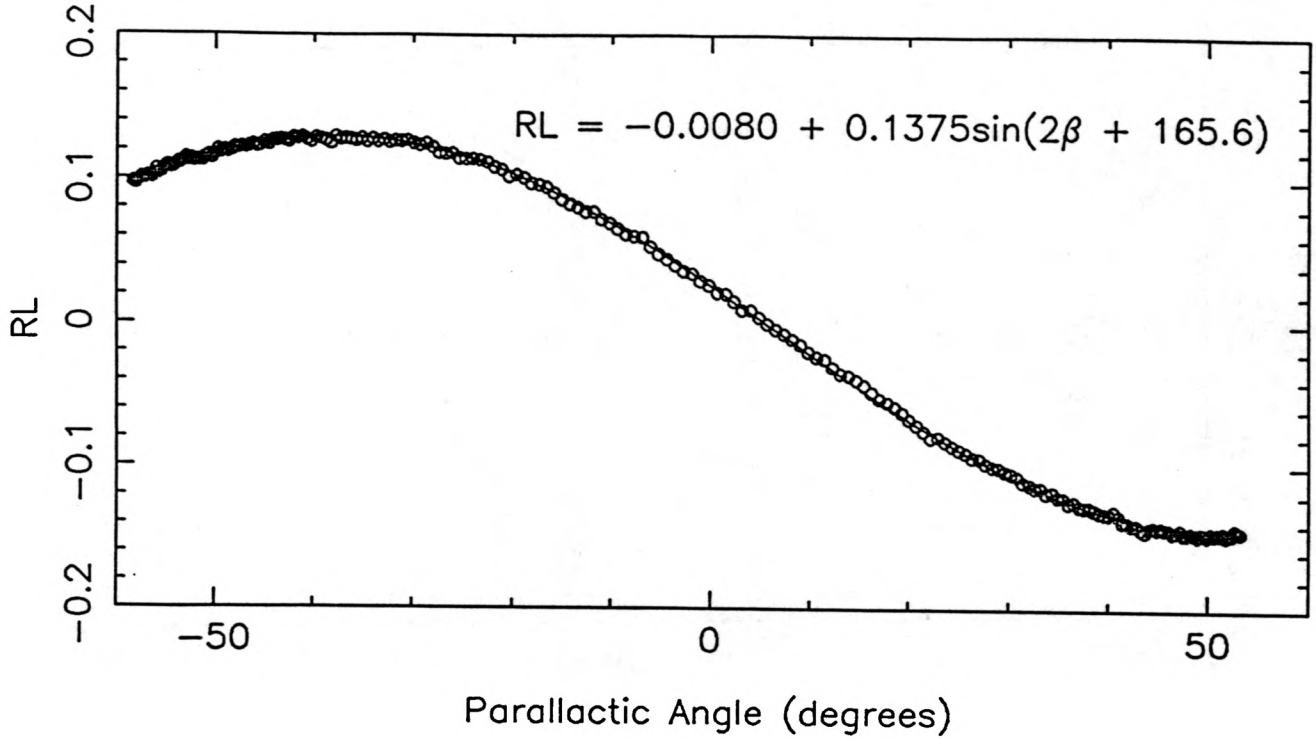

Figure 4d: Real Part of Cross Products (LR) for 3C286

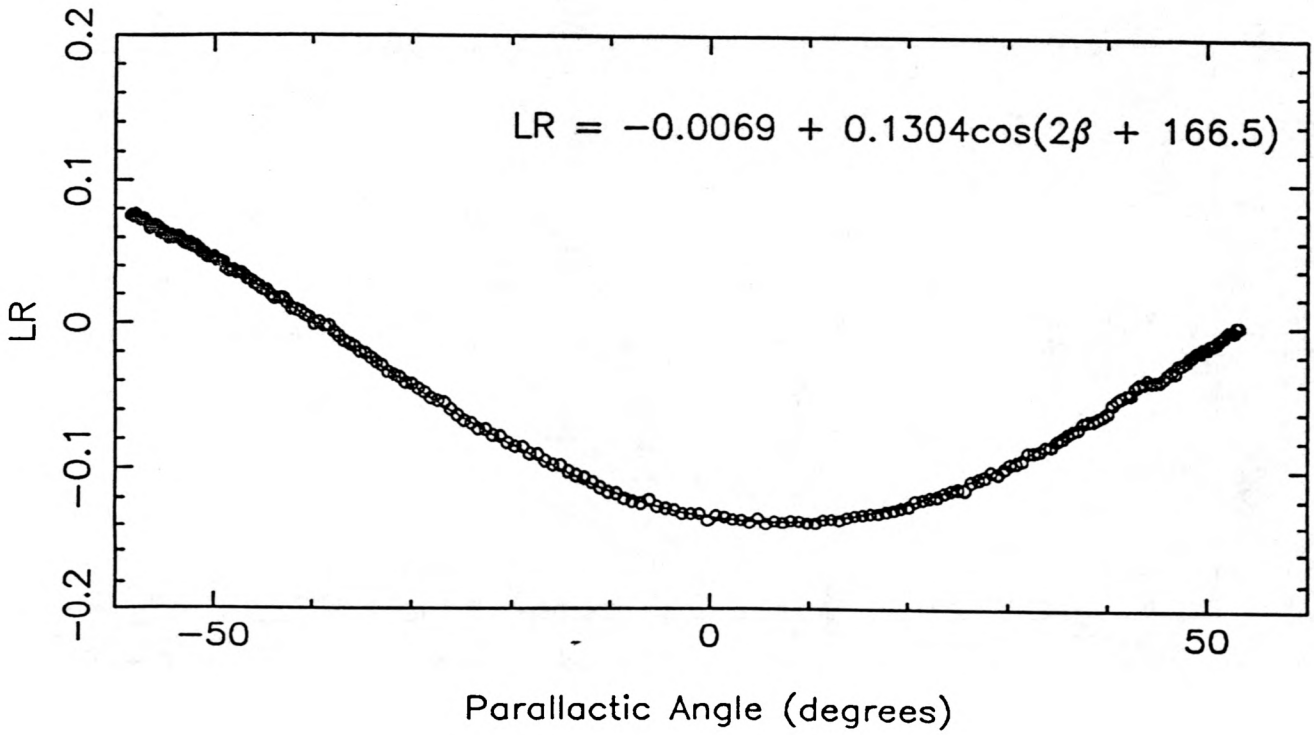

plots are the non-linear least squares best fits to the data. The circles in the data represent the actual data points, and the solid lines are the fits. As one can see from the equations, the amplitudes and phase offsets of the two sinusoids are nearly the same. The sinusoids are out of phase by almost 90 degrees. The constant offsets in both equations are very small. These conditions verify implication #2 and suggest $\psi_{RL} = \psi_{LR}$ which is a condition of implication #3. Since 3C286 has no circular polarization ($V = 0$) and is 11% linearly polarized, one can calculate $B_{RL} = 0.1375/0.11 = 1.25$ and $B_{LR} = 0.1304/0.11 = 1.19$. These values of B_{RL} and B_{LR} give $\sigma \sin(\psi_+ + \psi + \psi_{RL}) = 0.0064$ and $\sigma \cos(\psi_+ + \psi + \psi_{LR}) = 0.0058$. So, only sources of large flux (I) will contribute significantly to the constant offset in RL and LR. The RL instrumental phase angle, $\psi + \psi_{RL}$, may be calculated using the definition of θ from Section II and knowing the polarization angle of 3C286 at X-band ($2\phi = 65^0$). From the equation for RL in Figure 4c and equation 34, $2\beta + 165.6 = 2\beta - (65 + \psi + \psi_{RL})$, which gives $\psi +_{R\ \ L} = -230.6$. Since $\sin\theta = \sin(\theta + 2\pi), \psi + \psi_{RL} = 360 - 230.6 = 129.4$. Similarly for $LR, \psi + \psi_{LR} = 128.5$.

Figures 5a and 5b are plots of equations 38 and 39, respectively, versus parallactic angle for 3C286. The data have been corrected for gain and are normalized to the flux of 3c286. Recall the expressions for I_c and V_c assume the detectors are ideal. The figures show that I_c is essentially one and V_c is zero as they should be. A slight hint of sinusoidal variation is present in the plots with amplitudes of about one percent. This suggests an upper limit on δ and σ of about 10% since $P = 0.11$. δ and σ are probably much less than 0.10 because the data scatter in the figures is dominated by atmospheric phase instability.

Now that the amplitudes and phases of the complex gains and leakage factors are known, one may measure the polarization properties of other sources. Four VLA calibrators were observed during the February 14 run in addition to 3C286. With the exception of 3C286, each calibrator was observed for about 15 minutes. The flux (I), linear polarization (P), and polarization angle (2ϕ) calculated for each source are tabulated in Table A along with their associated one sigma errors. The source name is specified with J2000 terminology. The alias in Table A is an alternate source name. Sources which do not have 3C catalog numbers are denoted by their J1950 names.

Table A. Analog Sum Polarization Calibration.

Source(J2000)	Alias	I(Jy)	P(Jy)	2ϕ(deg)
1331+305	3C286	5.20 ± 0.04	0.57 ± 0.01	64.8 ± 0.9
1221+282	1219+285	1.07 ± 0.01	0.03 ± 0.01	-115.0 ± 11.2
1256-057	3C279	9.98 ± 0.09	0.14 ± 0.01	-114.2 ± 2.6
1229+020	3C273	25.20 ± 0.23	1.15 ± 0.02	-55.0 ± 0.8
1613+342	1611+343	3.01 ± 0.02	0.08 ± 0.01	12.2 ± 3.0

The results of the analog sum polarization calibration method were compared to those of standard interferometer polarization calibration. The interferometer results are tabulated in Table B.

Figure 5a: Measured Stokes I

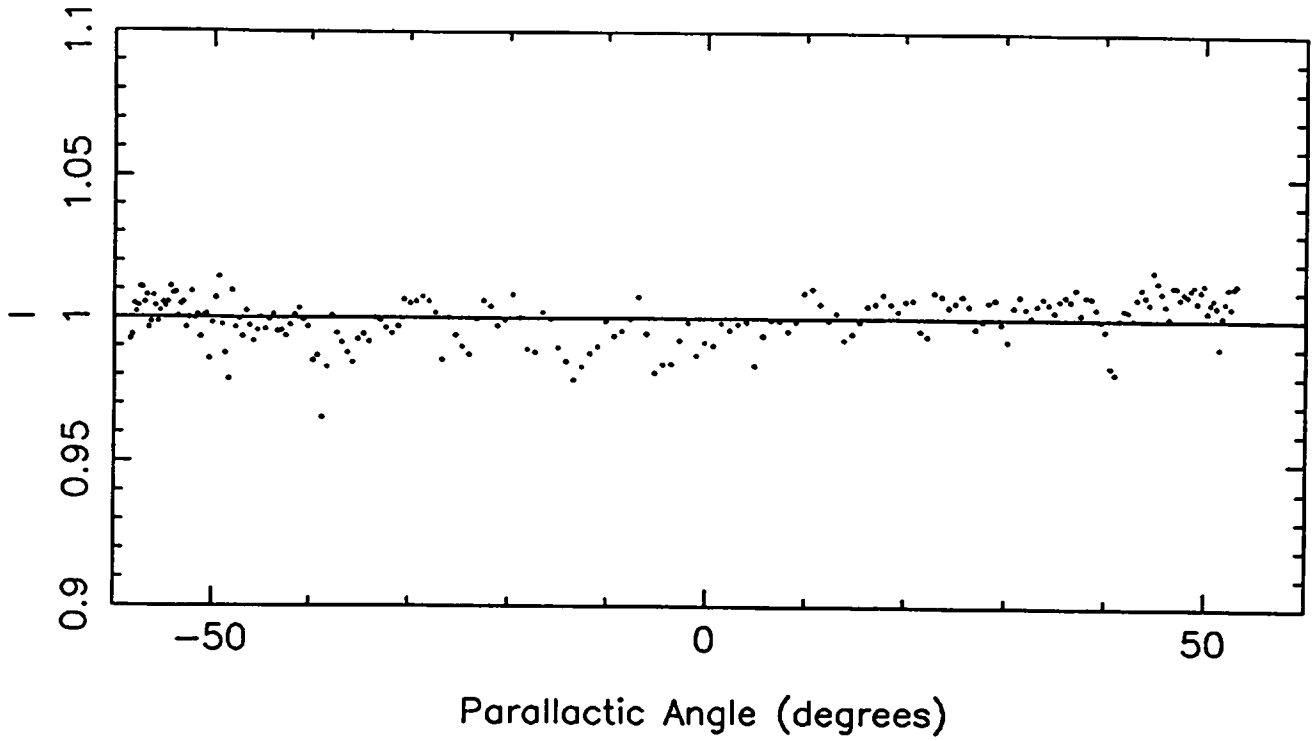

Figure 5b: Measured Stokes V

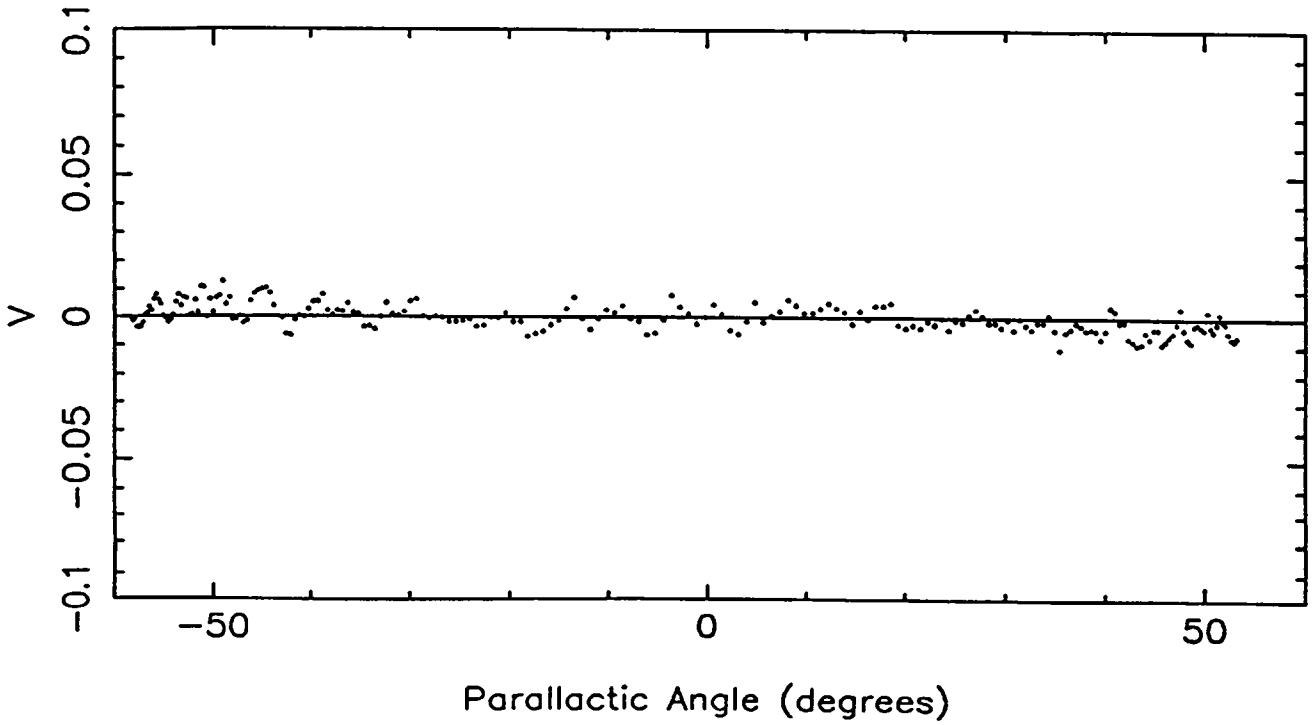

Table B. Interferometer Polarization Calibration.

Source(J2000)	Alias	I(Jy)	P(Jy)	2ϕ(deg)
1331+305	3C286	5.04 ± 0.11	0.58 ± 0.03	65.0 ± 0.1
1221+282	1219+285	1.02 ± 0.01	0.02 ± 0.01	-151.0 ± 3.6
1256-057	3C279	9.83 ± 0.12	0.12 ± 0.04	-160.6 ± 3.7
1229+020	3C273	25.90 ± 0.42	0.93 ± 0.19	-47.0 ± 0.5
1613+342	1611+343	2.90 ± 0.02	0.07 ± 0.02	-6.7 ± 0.8

The total and polarized fluxes in the two tables generally agree very well. Only the polarization angle of 3C286 is in good agreement between the two polarization calibration methods. Possible origins of the discrepancy in the polarization angle are atmospheric phase instability, discrepancies in the polarization calibration methods, and non-linear phase response of the HTRP to changing input power levels. Testing of the prototype HTRP detector set shows that the measured phase remains constant at intermediate input power levels (1990, McKinnon). Therefore, non-linear phase response cannot account for the discrepancy. The polarization calibration tests were performed under the worst of conditions for atmospheric phase stability: X-band in A array in wet weather. Testing of this polarization calibration method should be repeated under the more ideal observing conditions of lower frequency (L-band), smaller array configuration (C or D), and dry weather.

At some point, the two polarization calibration methods will not agree. When interferometer data is calibrated, one has the luxury of reviewing data from antenna pairs. If antenna data is corrupted, it may be removed from the data set. In the case of the analog sum, antenna data is summed in hardware regardless of the data quality. Therefore, the signal-to-noise ratio of the calibrated analog sum data will generally be worse than that of the calibrated interferometer data.

VI. HTRP Instrumental Response.

No instrument is perfect, and it is obviously important to understand the sources of error in the instrumentation. One channel of the HTRP phase shift/detector/integrator network was tested over its 4MHz design bandwidth to evaluate its performance. The following paragraph discusses the testing procedure.

The output of a frequency synthesizer was split by a power divider into the two HTRP inputs (R and L). The RR, LL, RL, and LR outputs of the HTRP were recorded for input frequencies of 0.2 to 4MHz at 0.2MHz intervals. The power out of the synthesizer was measured with a power meter to insure constant input power over the frequency range of the test. Occasionally the amplitude of the synthesizer waveform had to be adjusted to maintain constant signal power to the HTRP. The power was maintained at a level such that the power level into each HTRP input was -10dBm. The HTRP was designed to

Fig. 6a: RR Frequency Response

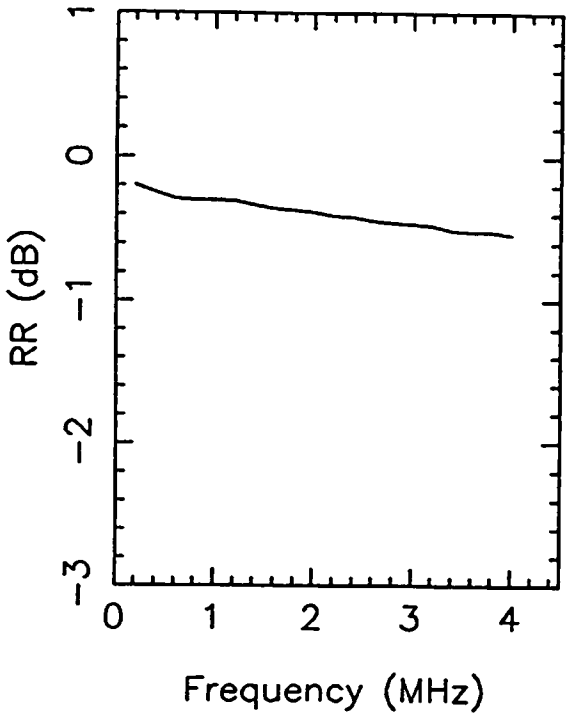

Fig. 6b: LL Frequency Response

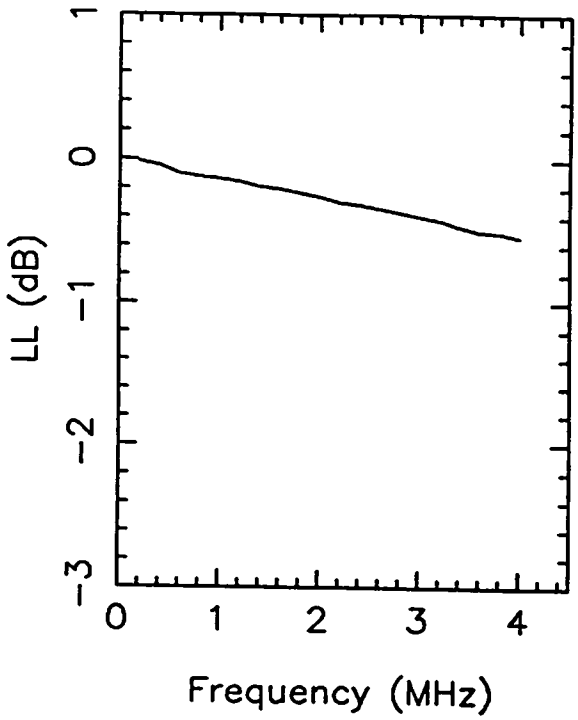

Fig. 6c: Cross Product Phase Error

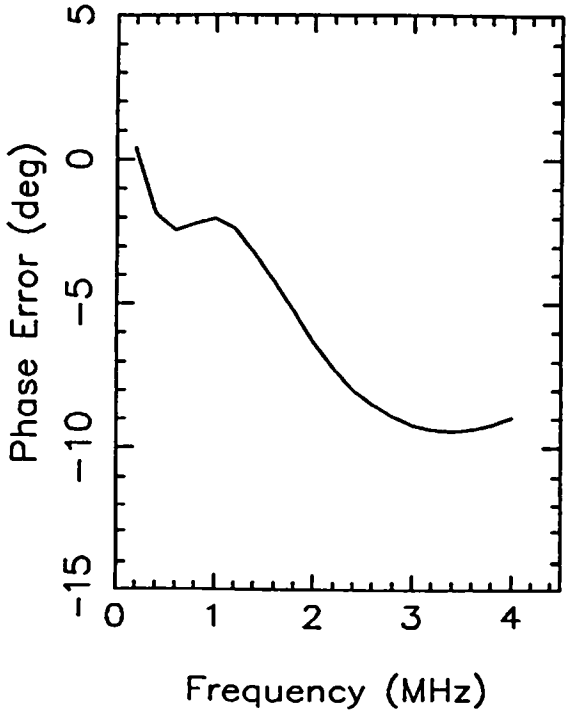

Fig. 6d: Integrated Phase Error

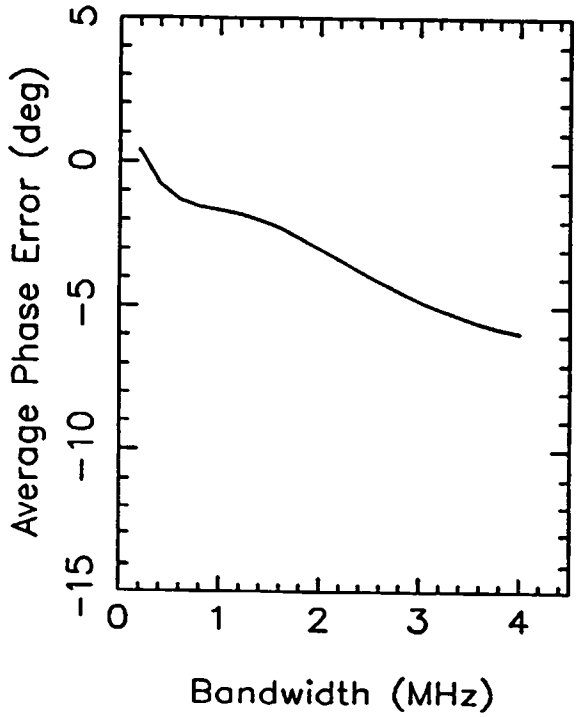

produce a one volt output for a -10dBm input. The power divider did not introduce a phase error in the cross products because it was made of resistors.

Ideally this test should produce one volt outputs at RR and LL. In terms of decibels (dB $= 10\log_{10}(V/V_o)$), the RR and LL outputs should be zero over the 4MHz frequency range. Since the R and L inputs were exactly in phase ($\theta = 0$), the LR output should have been one volt and the RL output should have been zero volts. The phase error over the frequency range would then be zero because $\theta = \arctan(RL/LR) = 0$. The actual results are shown in Figures 6a through 6d. The responses of the RR and LL detectors decline by about 0.6dB over 4MHz in Figures 6a and 6b. The phase error between RL and LR at a particular frequency is shown in Figure 6c. The phase of RL generally *lags* that of LR over the entire 4MHz range, and the phase error is as much as -9.4 degrees at 3.4MHz. Figure 6c is the phase error at a particular frequency component, but what is the phase error due to a broad band noise source? An estimate of the broadband phase error is the average of the function in Figure 6c over the corresponding frequency range. For a continuous function, the average is

$$\langle\theta\rangle_f = \frac{1}{f}\int_0^f \theta(\nu)d\nu \tag{44}$$

which shall be approximated in this case by

$$\langle\theta\rangle_f = \frac{1}{f}\sum_{i=0}^{i=f} \theta_i \Delta f \tag{45}$$

The incremental frequency, Δf, in the summation is 0.2MHz. Figure 6d plots the average phase error at each bandwidth, f. The effect of averaging over the band smooths the original function of Figure 6c. The largest phase error, -5.9 degrees, is expected to occur for an observation using a 4MHz bandwidth. For the observations discussed in Section V, the phase error at 1MHz is expected to be -1.6 degrees. From the equations for RL and LR in Figures 4c and 4d, the actual phase error is $165.6 - 166.5 = -0.9$ degrees. The agreement between the predicted and measured phase error is good considering the coarseness of the calculation in equation 45.

The non-ideal behavior of the detectors shown in Figure 6a through 6d justifies the need for the detector complex gains introduced in Section III. At larger bandwidths, the detector complex gain amplitude decreases and the phase error increases. Test observations at 4MHz support this hypothesis. The phase error at larger bandwidths causes polarization calibration to be more computationally intensive. Instead of calculating a phase from RL and LR and subtracting a single instrumental phase angle, one must individually correct RL and LR for their separate instrumental phase angles, and then compute the source polarization angle.

VII. Conclusions.

The polarization calibration scheme I have presented is applicable to observations of point sources at wavelengths where good polarization calibrators exist. Good polarization calibrators have constant polarization angle and polarized flux, and can be used to determine the absolute polarization angle of an arbitrary source. There are no good P-band

polarization calibrators for the VLA. One may still conduct P-band polarization observations to determine I, P, V, and relative polarization angle, but absolute polarization angle cannot be measured. I have not discussed Faraday rotation, and one must remember to account for Faraday depolarization by correcting the polarization angle. The results I have presented are encouraging, but they should be regarded as preliminary until additional testing of the HTRP is conducted at low frequency in a small array configuration.

VII. References.

Conway, R. G. and Kronberg, P. P., 1969, MNRAS, 142, 11.

Jackson, J. D., 1975, Classical Electrodynamics, John Wiley and Sons, New York.

Kraus, J. D., 1966, Radio Astronomy, McGraw-Hill, Inc., New York.

McKinnon, M. M., 1990, HTRP Memo: Allowable Operating Ranges for the HTRP (in prep).

Stinebring, D. R., 1982, PhD Thesis, Cornell University.